Journal of Nano Research Vol. 9 (2010) pp 101-108
Online available since 2010/Feb/15 at www.scientific.net

doi:10.4028/www.scientific.net/JNanoR.9.101

Synthesis and Characterization of NiCr Self-assembled Nanorings

Victor M. Serdio[1, a], Miguel A. Gracia-Pinilla[2,3,b], S. Velumani[4,c], Eduardo G. Perez-Tijerina[2,3,d] and Wilfred G. van der Wiel[5,e]

[1]Department of Physics, Tecnológico de Monterrey - Campus Monterrey, Nuevo Leon, C.P.64849, Mexico

[2]Laboratorio de Nanociencias y Nanotecnología - Facultad de Ciencias Físico Matemáticas Universidad Autónoma de Nuevo León, Monterrey, Nuevo León, 66450, México

[3]Centro de Innovación, Investigación y Desarrollo en Ingeniería y Tecnología (CIIDIT) Universidad Autónoma de Nuevo León, Apodaca, C.P.66600. Nuevo León, Mexico

[4]Department of Electrical Engineering (SEES), Cinvestav, Zacatenco, Av IPN 2508, Mexico city, C.P.07360, D.F. Mexico

[5]Strategic Research Orientation NanoElectronics, MESA+ Institute for Nanotechnology, University of Twente, P.O. Box 217, 7500 AE Enschede, The Netherlands

[b] miguel.graciapl@uanl.edu.mx

Received: June 19, 2008; revised: September 28, 2009; accepted: December 14, 2009

Keywords: NiCr, magnetic data storage, nanoparticles, size selected, inert gas condensation

Abstract. Formation of NiCr nanorings out of 2-3 nm NiCr nanoparticles prepared by DC magnetron sputtering with inert gas condensation is reported. An RF quadrupole mass filter has been used to get the particle size distribution and control the particle size in the plasma stream of grown material. The depositions are made on silicon substrates at room temperature under a helium and argon atmosphere of varying composition. By optimizing the He-Ar composition, magnetron power and the condensation zone, the particle size distribution is narrowed. Magnetic characterization determines that every single nanoparticle possesses a single magnetic domain that influenced their arrangement on the substrate. These arrangements were particularly in ring like structures. Particles join together while being deposited to form rings with a ~100 nm diameter. Particle density and agglomeration phenomena depend on the substrate's time of exposure to the NiCr nanoparticle source coming from the target.

Introduction

Bulk NiCr is a non-magnetic alloy (Ni80:Cr20) known for its high melting temperature and corrosion resistant qualities [1-3]. NiCr have been used as a heating element in various industrial applications due to its electrical properties. At the nanoscale, NiCr thin films have a low temperature coefficient of resistance (TCR) and a large resistivity [4], contrary to its properties at larger scales. Researchers have reported that Ni and Cr crystals in the case of specimens annealed in air, form oxides such as Cr_xO_y or Ni_jO_k which provides a reduction of the grain distribution and uniform pore structure in stable condition [5]. Many metal coating fabrication techniques like atomic layer deposition, physical and chemical vapor deposition have been developed over the years, but magnetron sputtering has certain advantages in conserving the composition of the deposition material. Many industrial Ni based coatings are being changed from conventional plating to sputtering because of the improvement in crystal structure. Ni based alloys can be deposited by this technique and have shown superior resistance to pitting corrosion in NaCl acidic solution [6] and are also of interest as fuel cell components due to its wide range of applications, as a catalyst in solid oxide fuel cells [7], hydrogen storage in the Ni-metal hydride battery [8], etc. Thin-film coatings were investigated by Navabpour *et al.*[9] for the adhesion of low-density polyethylene

(LDPE). Eight different samples were deposited by magnetron-sputtering over stainless steel substrates. NiCr coating showed one of the best results having no adhesion to the polymer, making this thin film perfect for LDPE processing tools.

Ni-based nanoparticles (NPs) have been investigated for a long time and show important advantages in ferrofluids, contrast enhancement in magnetic resonance imaging, and magnetic carriers for drug targeting [10]. An application of NiCr nanoparticles was developed by Kyung *et al.* [11]. They were able to grow carbon nanotubes and reported that, depending on the thickness of sputter deposited NiCr films the growth rate of carbon structures varied and the yield was maximum at 10 nm thickness. These second phase particles were purposely introduced to act as a catalyst, to direct and confine the CNTs growth into an area determined by the size of the particle. Magnetic memory storage applications have been the most widely studied area. Ni and NiO monodispersed magnetic nanoparticles are able to organize and self-assemble into 2D and 3D superlattice structures [10]. This behavior is advantageous for the use in magnetic data storage and electronic devices [10]. NiCr thus combines self-assembly potential with ferromagnetic behavior, as required for magnetic data storage applications.

Recently, the formation of nanorings has been reported for different materials and dimensions with valuable properties for magnetic memory storage. Combinations of Co, Cu, NiFe (80:20), Si, or GaAs have been successfully tested for the synthesis of these formations [12-15]. Although many compositions of nanorings have been reported, they all have in common the process of lithography in one of their nanoring preparation steps. Tripp *et al*. [16] have developed self-assembled magnetic nanorings that consist of a few 27 nm Co particles and have a diameter of less than 100 nm. The formation takes place when the particles acting as magnetic dipoles link up into a ring forming a closed circuit, which minimizes the magnetic energy and the field outside the ring. Magnetic rings are considered as a candidate for binary data storage because their magnetostatic fields can be entrained into chiral domains that can be magnetized clockwise or counter clockwise, representing the two possible magnetic states of the ring [16].In this article, we present the synthesis and characterization by inert gas condensation (IGC) DC-magnetron sputtering of magnetic NiCr self-assembled nanorings on Si and glass substrates. The single NPs that form the nanorings are composed of NiCr nanoparticles with average size of 2-3 nm. The nanorings have the same height (~2 nm) and an average diameter of 130 nm.

Experiment

The NiCr NPs are produced in a Nanogen 50 system (Nanoparticles source) by Mantis Deposition Ltd. [17] , using the IGC [18-20]. A supersaturated vapor of metal atoms is originated by sputtering of NiCr (80:20) alloy target in an inert gas atmosphere of Ar and He. The Nanogen system is cooled by circulating a coolant mixture based on water. The preparation process starts when the Nanogen and deposition chamber are evacuated down to $\sim 10^{-8}$ torr. After reaching the desired vacuum level, inert gases are introduced to the Nanogen and deposition chamber until a partial pressure of $\sim 10^{-1}$ torr. The composition of this atmosphere is a key factor in the experiment because the size, distribution, and density of NPs are controlled through the variation of Ar and He gas flow. The sputtering unit's magnetron is optimized to work in a power range of 50-60 W, and the condensation zone length between 0 - 10 cm. The quadrupole spectrometer mass filter is activated to characterize particles sizes at the plasma beam before deposition. The quadrupole mass filter utilizes a DC and RF voltage that enables one to monitor the mass spectrum and to filter an optimized particle size. For NiCr, a frequency of 20 kHz displays the complete nucleation particle size distribution in the plasma. Amplitude of the signal allows selecting a certain particle diameter along the curve and filter them. In Fig. 1 it is shown how the optimization of gas composition was carried out. Compositions of 10 sccm of Ar and 15 to 25 sccm of He are concluded to be most favorable for the synthesis.

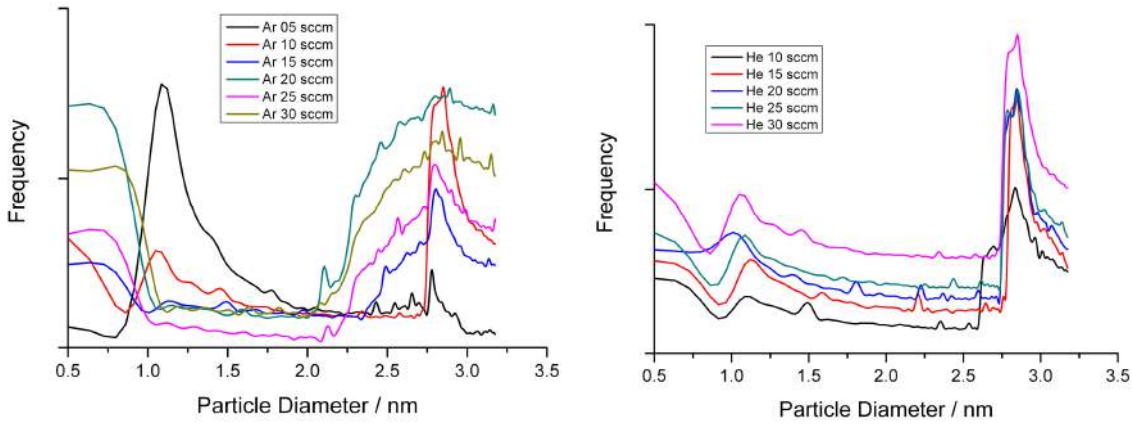

Fig. 1. NiCr nanoparticles mass filter's spectra, for Argon optimization 25 sccm of Helium were used and for Helium optimization 10 sccm of Argon. Y-axis are arbitrary units, curves in Helium optimization have different set points for better visualization.

The particles are deposited on a Si substrate having the quadrupole spectrometer mass filter set for a certain particle size optimization. Some of the depositions are carried out without the filter, because sometimes the desired particle size and distribution were already achieved without filter, solely by varying the gas composition. All depositions without mass filter are made for a maximum of 5 minutes, while depositions with filtered particles take 25~40 minutes. NP density is controlled by the deposition time. Structural and morphological properties of NPs accumulated on the substrate are manipulated using a technique called energy cluster impact (ECI) [21-22]. For all depositions the energy of impact is set to ~0.1eV/atom to achieve a "soft landing" of particles over the substrates. Using these experimental characteristics it is possible to retain the structural properties of Nps generated in the system nanogen 50 [23-25].

The characterization of NPs on the substrate is performed with a Veeco Instruments multimode scanning probe microscope by hard tapping (low amplitude set point voltage) mode in atomic and magnetic force microscopy (AFM & MFM). Because of the expected NP characteristics, a 10 μm scanner was selected for the analysis. The AFM analysis is performed in order to obtain the characteristics (diameter, height) of single NPs and statistical data of NP ensembles. Magnetic domains imaging and magnetic properties of the NPs are confirmed by the MFM analysis.

Results and Discussion

The dispersed NiCr NPs are observed in Fig.2 and the statistical size distribution of nanoparticles is shown in Fig. 3. NPs conserve a similar structure and uniform distribution over large areas of the NiCr covered substrate. Monodispersed NP sizes and particle analysis were carried out for each of the early samples with the same fabrication conditions. In Fig. 1 it is observed that with or without the activation of filter, the beam was formed primarily by particles with a ~3 nm diameter; nevertheless after obtaining the statistical analysis of data over several samples of depositions on silicon substrates as seen in Fig. 3 a) and b), the results showed that the particles deposited have a mean diameter of 11 nm and height of 2 nm. This fact proves that the "soft landing" is partially achieved and helps us to conclude that Volmer-Weber growth [26] was developed among the depositions, which yielded a narrow NP size distribution. This kind of behavior is a result of the strongly bonded NiCr species and a weak bonding to the semi-conducting Si substrate.

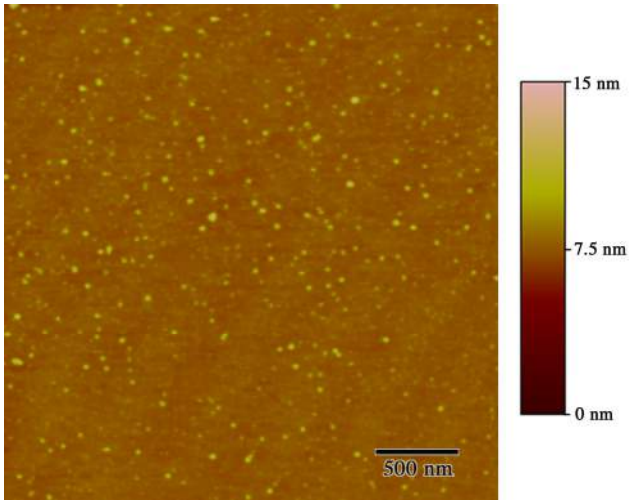

Fig. 2. AFM image in topographic mode of monodispers NiCr nanoparticles deposited in Si substrates at room temperature.

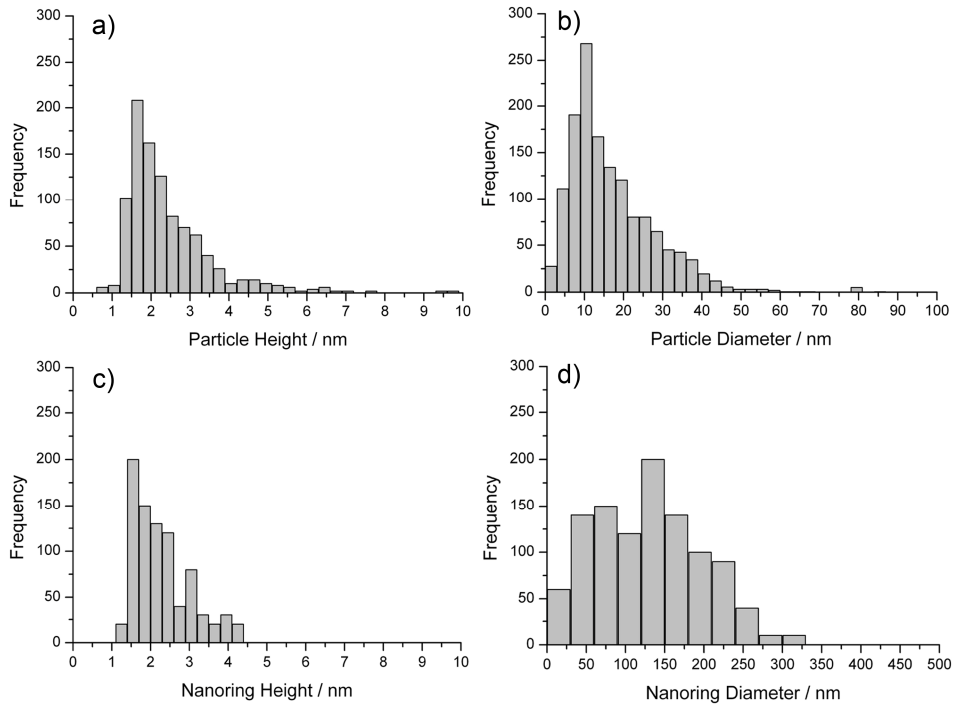

Fig. 3. Statistical analysis of particles (a and b) and nanoring (c and d) sizes.

To characterize the magnetic properties of NPs, MFM analysis is used. The specific values in the interleave scan height and drive amplitude play a key role in this characterization, the interleave scan height was decreased and the drive amplitude was increased to the maximum, but avoiding contact with the sample. Mean diameter of particles along the study of several depositions was 10 nm, but small quantity of aggregates of nanoparticles with a diameter of ~40 nm were also observed in different regions of the sample. Magnetic imaging of particles smaller than 10 nm was difficult to achieve due to the small magnetic force interactions between the tip and sample. That is why one of the larger particle areas was selected to obtain enough contrast of the particle's domains. The magnetic domains can be detected in the frequency scan either as holes or peaks, depending on the direction of magnetization. Each of these holes or peaks represent a particle made up by a single or a preferential arrangement of many magnetic domains in the same direction, so each nanoparticle is

considered to possess a single direction of magnetization, hence forming a magnetic dipole. Generally, in a bimetallic ferromagnetic dispersed nanoparticles deposition it's expected to have a different magnetic orientation for each particle because a preferential orientation was not controlled and they are randomly deposited on the substrate, but as it is observed in Fig. 4, all the particles are represented by a dip in the frequency image. This singularity is a common phenomenon in MFM analysis and this happens when the tip's magnetic field is larger than the coercive field of the material and thus particles are magnetized. Magnitude of this field depends on the magnetic properties of each material. That is why in this scan, all the particles possess the same direction of magnetization.

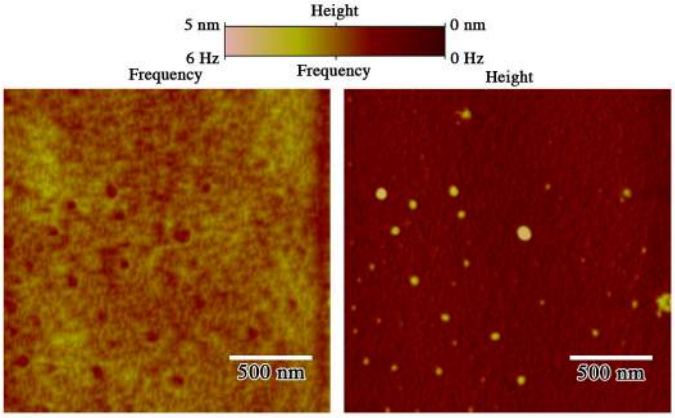

Fig. 4. AFM and MFM images, frequency and height images of the same scan area. These measurements were made at room temperature. (the scale bar is 500nm).

In other experimental conditions nanoparticles self-assembled into ring-like formations with an average diameter of 130 nm and a narrow distribution over larger areas has been observed (Fig.5a). This behavior is conserved all over the substrate. Similar behavior was previously reported with magnetic dipole Co NPs [16], where it was proved by transmission electron microscopy and electron holography images that the particles became aligned into a loop to produce a zero net moment, which minimized the magnetic energy and the field outside of the ring structure. The breakthrough in the synthesis of NiCr nanorings is that in the deposition only ring structures were found, nearly no single particles were identified. Nanorings were successfully reproduced in other experimental deposition conditions with small differences in their uniformity and distribution (Fig. 5b). These differences are attributed to the slight variations in synthesis parameters and the geometric changes of the surface in the NiCr sputtering source target. One of the differences was the decrease in cohesion (adsorption energy) of the particles, but this defect helped in understanding the formation of rings because it contrasted each of the single nanoparticle forming the ring, emphasized the arrangement and proved how single 10 to 20 nm diameter aggregates self-assembled into ring formations.

In the formation of the ring-like structures, NiCr NPs are influenced by the bonding forces (Van der walls, London forces, Keeson forces, Debye forces) among each other in the nucleation process, the magnetic interactions exhibited is suggested to be the central cause for this shaping phenomenon. The "soft landing" provided sufficient mobility to particles and enabled the influence of interactions between particles in the formation of structures within the substrate. Particle-particle magnetic interactions acted as the mechanism (forces or dipole-direct self-assembly) that diminished the superficial energy, while the particle-substrate interactions were only the adherence provided by the bias voltage between the substrate and NiCr target.

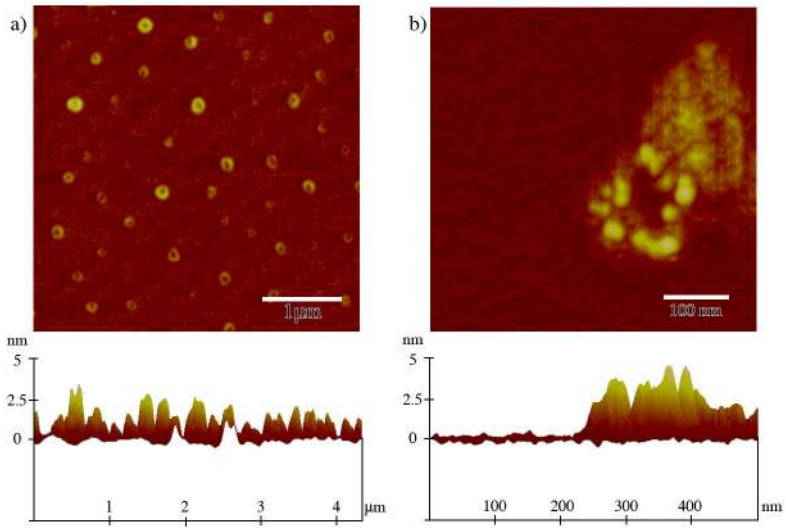

Fig. 5. a) . Large area at Monodispers of self-assembled nanorings with mean diameter of 130 nm, b) Zoom in of one 120 nm diameter nanoring with slight synthesis variation. The bar scale are at left 1μm and right 100nm.

The cyclic assembly of NPs (acting as magnetic dipoles) forms a ring structure that produces a magnetic flux closure domain. This property is ideal for data storage applications because this allow the ring to have two possible states (binary) in the alignment of the magnetic dipoles in the rings, clock-wise or counter clock-wise. Grain size and particle analysis was also performed for the deposited nanorings to yield statistical data about their dimensions in Fig. 3 c) and d). In both nanorings depositions, the height of ~2 nm was conserved (Fig. 5 and 3), which also agrees with the mean height of the single NPs depositions as shown in Fig. 3 a).

Fig. 4 shows the magnetic property for smaller particles with size around 3nm, while Fig 6. gives the morphological and magnetic properties for larger particles with sizes in the range between 20 and 500nm. We can see the new self-assembling of NiCr nanoparticles large rings, the principal difference with the first ring (view fig. 5.) is the size and the distribution of particles inside the rings. In the first case the ring is formed from the same size of particles, in this case the ring is formed by one large aggregate in the center surrounded by small particles that shows a ring arrangement. We propose that this configuration is formed due the high mobility of the particles and posterior ensemble generated by different interactions between the particles such as the particle-particle magnetic interactions (forces or dipole-direct self-assembly).

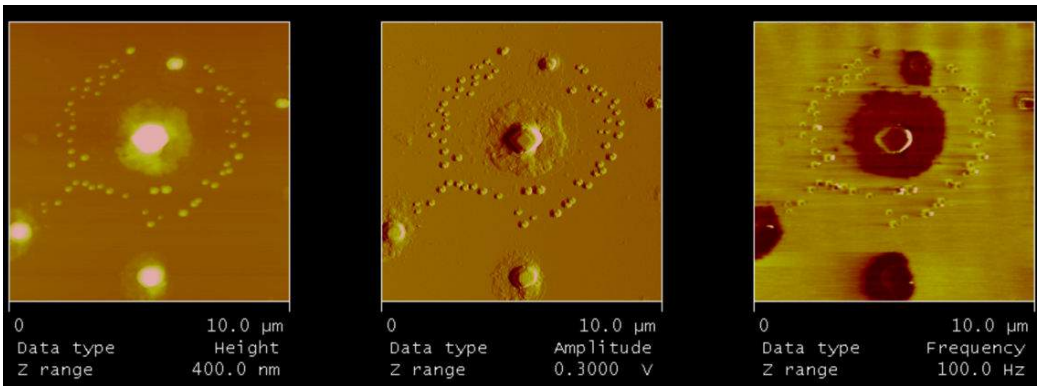

Fig. 6. AFM and MFM images, height, amplitude and frequency images of the same scan area. These measurements were made at room temperature.

Analyzing Table 1 it can be concluded that the key factors between fabricating a uniform nanoparticle deposition and nanorings deposition were the supply of power to the magnetron to create a sufficiently strong magnetic field over the sputtering source target, and low bias voltage to enable mobility of particles. The recipe for creating random arrangements of dispersed NiCr nanorings was already developed and documented. Even though nanorings are very delicate to synthesis, the self-assembly quality shows great advantages over other nanoring fabrication techniques. Future work will be dedicated into two important subjects; to modify the synthesis parameters to fabricate a coherent sequence arrangement of nanorings to be able to have an ordered line of rings to read and write data. The second is to determine the magnetic hysteresis curve of these nanostructures (magnetic properties) in order to have the magnitude of coercive field and reproduce this field with magnetic writing device.

Table 1. Synthesis conditions of the most relevant depositions in chronological order. Depositions number 2 and 9 presented nanorings.

#	Magnetron power supply (Watts)	Condensation zone (cm)	Bias voltage (V)	Deposition time (min)	Mass filter particle diameter optimization (nm)	Gas composition Ar – He (sccm)
1	57.12	13	60	2	None	10 – 25
2	57.12	0	60	2	None	10 – 25
3	50.08	0	59.2	2	None	10 – 25
4	50.08	13	59.2	2	None	10 – 25
5	44.48	0	110.1	20	2.83	10 – 10
6	54.201	6.5	59.5	25	5.02	45 – 0
7	48.16	0	60.9	2	None	10 – 25
8	48.48	0	60.9	3	None	10 – 25
9	60.652	0	60	5	None	10 – 25
10	69.148	0	111.2	30	2.36	10 – 25
11	68.44	0	111.3	6	2.97	10 – 25

Acknowledgments

We would like to thank Gerardo T. Martinez for his contribution to the AFM characterization. Also to the Monterrey Institute of Technology, to the Universidad Autónoma de Nuevo León for their support and several other research projects, and to the National Council for Science and Technology, Mexico (CONACYT), grant (207569).

References

[1] N. F. Ak, C. Tekmen, I. Ozdemir, H. S. Soykan and E. Celik: *Surf. Coat. Technol.* 174 (2003) 1070-1073.

[2] T.S. Sidhu, S. Prakash and R.D. Agrawal: *Surf. Coat. Technol.* 200 (18-19) (2006)5542-5549.

[3] S. Velumani, H. Castaneda, U. Pal, J. A. Chavez, P. J. Sebastian and J. A. Ascencio: *J. Solid State Electrochem.* 9(8) (2005) 535-546.

[4] G. Nocerino and K.E. Singer: *Thin Solid Films* 57 (2) (1979) 343-348.

[5] Y. Kwon, N. H. Kim, G. P. Choi, W.S. Lee, Y. J. Seo and J.S. Park: *Microelectronic Engineering* 82 (3-4) (2005) 314-320.

[6] L. Liu, Y. Li and F. H. Wang: *Electrochimica Acta* 52 (7) (2007) 2392-2400.

[7] B. F. Tu, Y. L. Dong, B. Liu and M. J. Cheng: J. *Power Sources* 165 (1) (2007) 120-124.

[8] E. Jankowska, M. Makowiecka and M. Jurczyk: *J. Alloys& Compounds* 404 (2005) 691-693

[9] P. Navabpour, D.G. Teer, D.J. Hitt and M. Gilbert: *Surf. Coat. Technol.* 201(6) (2006) 3802-3809.

[10] J. Park, E. Kang, S. U. Son, H. M. Park, M. K. Lee, J. Kim, K. W. Kim, H. J. Noh, J. H. Park, C. J. Bae, J. G. Park and T. Hyeon: *Advanced Materials* 17(4) (2005) 429.

[11] S. J. Kyung, M. Voronko, Y. H. Lee, C. W. Kim, J. H. Lee and G. Y. Yeom: *Surf. Coat. Technol.* 201(9-11) (2007) 5378-5382.

[12] C.A. F. Vaz, M. Klaui, J. A.C. Bland, L.J. Heyderman, C. David and F. Noltin: *Nuclear Instruments & Methods in Physics Research Section B-Beam Interactions with Materials and Atoms* 246 (1) (2006)13-19.

[13] M. Brands, A. Carl and G. Dumpich: *Superlattices and Microstructures* 37(6) (2005)388-393.

[14] Z. Cui, J. Rothman, M. Klaui, L. Lopez-Diaz, C. A. F. Vaz and J. A. C. Bland: *Microelectronic Engineering* 61-2 (2002) 577-583.

[15] J. Podbielski, F. Giesen, M. Berginski, N. Hoyer and D. Grundler: *Superlattices and* Microstructures 37(5) (2005)341-348.

[16] S. L. Tripp, R. E. Dunin-Borkowski and A. Wei: *Angewandte Chemie-International Edition* Vol. 42 (45) (2003), p. 5591-5593.

[17] Mantis deposition Ltd, Oxford, England. www.mantisdeposition.com.

[18] K. Sattler, J. Mühlbach and E. Recknagel: *Phys. Rev. Let.* 45(10) (1980)821-825.

[19] S. H. Barker, S.C. Thorton, A. M. Keen, T. I. Preston, C. Norris, K.W. Edmonds and C. Binns: *Rev. Sci. Instrum.* 68(4) (1997)1853-1857.

[20] I.M. Goldby, B. Von Issendorff, L. Kuipers and R.E. Palmer: *Rev. Sci. Instrum.* 68 (9) (1997) 3327-3334.

[21] H. Haberland, Z. Insepov and M. Moseler: *Phys. Rev. B* 51(16) (1995)11061-11067.

[22] O. Rattunde, M. Moseler, A. Häfeler, J. Kraft, D. Rieser and H. Haberland: *J. Appl. Phys.* 90(7) (2001) 3226-3231.

[23] E. Peréz-Tijerina, M.A. Gracia-Pinilla, S. Mejía-Rosales, Ortiz-Méndez, A. Torres and José-Yacamán: M. *Faraday Discuss* 138 (2008) 353-362.

[24] M. A. Gracia-Pinilla, E. Pérez-Tijerina, J. A. García, C. Fernández-Navarro, A. Tlahuice-Flores, S. Mejía-Rosales, J.M. Montejano-Carrizales and M. José-Yacamán, M: *J. Phys. Chem. C* 112 (2008) 13492-13498.

[25] (a) S. Stappert PhD. Thesis, Univertität Duisburg Dessen, (2003). (b) I. Shyjumon Ph.D. Thesis, University of Greifswald, (2005). (c) M. A. Gracia-Pinilla Ph. D. Thesis, Universidad Autónoma de Nuveo León, (2008).

[26] R. Koch, H. Dongzhi and A. K. Das: *Phys. Rev. Lett.* 94 (2005)146101.

Journal of Nano Research Vol. 9
doi:10.4028/www.scientific.net/JNanoR.9

Synthesis and Characterization of NiCr Self-Assembled Nanorings
doi:10.4028/www.scientific.net/JNanoR.9.101

References
[1] N. F. Ak, C. Tekmen, I. Ozdemir, H. S. Soykan and E. Celik: Surf. Coat. Technol. 174 (2003) 1070-1073.
doi:10.1016/S0257-8972(03)00367-0

[2] T.S. Sidhu, S. Prakash and R.D. Agrawal: Surf. Coat. Technol. 200 (18-19) (2006)5542-5549.
doi:10.1016/j.surfcoat.2005.07.101

[3] S. Velumani, H. Castaneda, U. Pal, J. A. Chavez, P. J. Sebastian and J. A. Ascencio: J. Solid State Electrochem. 9(8) (2005) 535-546.
doi:10.1007/s10008-004-0587-9

[4] G. Nocerino and K.E. Singer: Thin Solid Films 57 (2) (1979) 343-348.
doi:10.1016/0040-6090(79)90176-7

[5] Y. Kwon, N. H. Kim, G. P. Choi, W.S. Lee, Y. J. Seo and J.S. Park: Microelectronic Engineering 82 (3-4) (2005) 314-320.
doi:10.1016/j.mee.2005.07.040

[6] L. Liu, Y. Li and F. H. Wang: Electrochimica Acta 52 (7) (2007) 2392-2400.
doi:10.1016/j.electacta.2006.08.070

[7] B. F. Tu, Y. L. Dong, B. Liu and M. J. Cheng: J. Power Sources 165 (1) (2007) 120-124.
doi:10.1016/j.jpowsour.2006.11.058

[8] E. Jankowska, M. Makowiecka and M. Jurczyk: J. Alloys& Compounds 404 (2005) 691-693
doi:10.1016/j.jallcom.2004.09.084

[9] P. Navabpour, D.G. Teer, D.J. Hitt and M. Gilbert: Surf. Coat. Technol. 201(6) (2006) 3802-3809.
doi:10.1016/j.surfcoat.2006.06.042

[10] J. Park, E. Kang, S. U. Son, H. M. Park, M. K. Lee, J. Kim, K. W. Kim, H. J. Noh, J. H. Park, C. J. Bae, J. G. Park and T. Hyeon: Advanced Materials 17(4) (2005) 429.
doi:10.1002/adma.200400611

[11] S. J. Kyung, M. Voronko, Y. H. Lee, C. W. Kim, J. H. Lee and G. Y. Yeom: Surf. Coat. Technol. 201(9-11) (2007) 5378-5382.

doi:10.1016/j.surfcoat.2006.07.191

[12] C.A. F. Vaz, M. Klaui, J. A.C. Bland, L.J. Heyderman, C. David and F. Noltin: Nuclear Instruments & Methods in Physics Research Section B-Beam Interactions with Materials and Atoms 246 (1) (2006)13-19.
doi:10.1016/j.nimb.2005.12.006

[13] M. Brands, A. Carl and G. Dumpich: Superlattices and Microstructures 37(6) (2005)388-393.
doi:10.1016/j.spmi.2005.01.006

[14] Z. Cui, J. Rothman, M. Klaui, L. Lopez-Diaz, C. A. F. Vaz and J. A. C. Bland: Microelectronic Engineering 61-2 (2002) 577-583.
doi:10.1016/S0167-9317(02)00476-8

[15] J. Podbielski, F. Giesen, M. Berginski, N. Hoyer and D. Grundler: Superlattices and Microstructures 37(5) (2005)341-348.
doi:10.1016/j.spmi.2004.12.006

[16] S. L. Tripp, R. E. Dunin-Borkowski and A. Wei: Angewandte Chemie-International Edition Vol. 42 (45) (2003), p. 5591-5593.
doi:10.1002/anie.200352825
PMid:14639723

[17] Mantis deposition Ltd, Oxford, England. www.mantisdeposition.com.

[18] K. Sattler, J. Mühlbach and E. Recknagel: Phys. Rev. Let. 45(10) (1980)821-825.
doi:10.1103/PhysRevLett.45.821

[19] S. H. Barker, S.C. Thorton, A. M. Keen, T. I. Preston, C. Norris, K.W. Edmonds and C. Binns: Rev. Sci. Instrum. 68(4) (1997)1853-1857.
doi:10.1063/1.1147957

[20] I.M. Goldby, B. Von Issendorff, L. Kuipers and R.E. Palmer: Rev. Sci. Instrum. 68 (9) (1997) 3327-3334.
doi:10.1063/1.1148292

[21] H. Haberland, Z. Insepov and M. Moseler: Phys. Rev. B 51(16) (1995)11061-11067.
doi:10.1103/PhysRevB.51.11061

[22] O. Rattunde, M. Moseler, A. Häfeler, J. Kraft, D. Rieser and H. Haberland: J. Appl. Phys. 90(7) (2001) 3226-3231.
doi:10.1063/1.1398067

[23] E. Peréz-Tijerina, M.A. Gracia-Pinilla, S. Mejía-Rosales, Ortiz-Méndez, A. Torres and José-Yacamán: M. Faraday Discuss 138 (2008) 353-362.

[24] M. A. Gracia-Pinilla, E. Pérez-Tijerina, J. A. García, C. Fernández-Navarro, A. Tlahuice-Flores, S. Mejía-Rosales, J.M. Montejano-Carrizales and M. José-Yacamán, M: J. Phys. Chem. C 112 (2008) 13492-13498.
doi:10.1021/jp804085q

(a) S. Stappert PhD. Thesis, Univertität Duisburg Dessen, (2003).

(b) I. Shyjumon Ph.D. Thesis, University of Greifswald, (2005).

(c) M. A. Gracia-Pinilla Ph. D. Thesis, Universidad Autónoma de Nuveo León, (2008).

[26] R. Koch, H. Dongzhi and A. K. Das: Phys. Rev. Lett. 94 (2005)146101.
doi:10.1103/PhysRevLett.94.146101
PMid:15904079